LA-UR-18-20686
Approved for public release; distribution is unlimited.

Title: Sensitivity Analysis and Requirements for Temporally and Spatially Resolved Thermometry Using Neutron Resonance Spectroscopy

Author(s): Fernandez, Juan Carlos
Barnes, Cris William
Mocko, Michael Jeffrey
Zavorka, Lukas

Intended for: Milestone report addendum, distribution to colleagues for peer review.

Issued: 2018-01-31

Sensitivity Analysis and Requirements for Temporally and Spatially Resolved Thermometry Using Neutron Resonance Spectroscopy

Juan C. Fernández, Cris W. Barnes, Michael J. Mocko, and Lukas Zavorka
Los Alamos National Laboratory, Los Alamos, NM 87545
(Dated: January 30, 2018)

This report is intended to examine the use of neutron resonance spectroscopy (NRS) to make time-dependent and spatially-resolved temperature measurements of materials in extreme conditions. Specifically, the sensitivities of the temperature estimate on neutron-beam and diagnostic parameters is examined. Based on that examination, requirements are set on a pulsed neutron-source and diagnostics to make a meaningful measurement.

CONTENTS

I. INTRODUCTION AND REQUIREMENTS

For the study of the dynamics of materials subjected to transient extreme conditions, bulk thermometry is a critical unmet scientific need. The temperature of a material is an independent thermodynamic variable in the equations of state. Thermometry is thus needed for full validation of theoretical models. It is not just the surface temperature, but the temperature and its gradient across the entire sample that are desired.

Requirements for temperature measurements to meet the established mission need of the MaRIE project have been analyzed.[1] The expected range of material temperatures is 300–3000 K, and the desired accuracy is ≈ 25 K or 2% (whichever is greater). While faster and better resolution help, the threshold requirement for the project would be internal temperature measurements with 100 μm spatial and 100 nsec temporal resolution. With such a measurement coupled with other diagnostics from the surface, volumetric temperatures can be modeled and theories challenged and validated.

Current dynamic temperature measurements have many drawbacks.[2] They may only be able to measure the surface temperature of a visibly opaque material, as in the case of pyrometry. They may be perturbative as with thermocouples. With techniques based on x-ray scattering, such as Thomson scattering, the beam may not penetrate sufficiently into samples that are thick or have high atomic number. In other cases, such as with the Debye-Waller effect, the technique is only applicable to crystalline samples.

Volumetric temperature measurements using neutron resonance scattering or spectroscopy have been demonstrated for static[3–8] as well as for shock-loaded samples,[9] where the high penetration of thermal and epithermal neutrons and mature neutron time-of-flight diagnostic techniques are exploited. For these reasons such a technique is being considered as a diagnostic to meet MaRIE requirements, possibly in concert with other techniques utilized simultaneously, such as pyrometry. For example, a concern with pyrometry is the modeling necessary to turn the measured surface emission into an interior temperature. NRS thermometry could validate such modeling to simplify further experiments in a series. Moreover, the measurement is robust. Swift *et al.*[10] pointed out that "NRS is inherently far less sensitive than emission spectrometry to heterogeneities in the temperature, because the width of the NRS peak is proportional to T, whereas thermal emission is proportional to T^4."

A. The Principle of NRS

Neutrons are absorbed by many isotopes at well-defined neutron energies (absorption resonances) above $\sim$1 eV. The lowest resonance energies for a given nucleus are generally highest for the lightest elements, and typically lie in the epithermal energy range for metals such as Zr and heavier. The natural resonance width increases by Doppler broadening, *i.e.*, the cumulative Doppler shifts of atoms in thermal motion. If the natural width is suffi-

ciently narrow relative to the Doppler broadening, which is usually the case except for the lightest elements, the increase in width may be used to measure temperature, as demonstrated by several groups[3–9]. Moreover, if the sample as a whole is moving sufficiently fast along the probe direction (*e.g.*, when shocked), that speed can also be measured by the overall shift in the resonance. The thermal motion depends on the atomic environment of the nucleus. In a gas it is straightforward to account for that environment with a Maxwell-Boltzmann (MB) distribution, but in the crystalline solid is an overlay of phonon modes. Therefore the resonance may appear differently in metallic uranium, uranium oxide, or UF_6 gas and therefore it is sensitive to phase transformation. In general, the higher the sample temperature is relative to the Debye temperature θ_D of the solid (see definition and typical values below), the less sensitive the resonance profile is to these effects. Since epithermal neutrons penetrate cm-scale lengths in all materials, NRS is truly a bulk temperature measurement method.

The NRS measurement is done by directing a source of neutrons with a broad energy distribution at a sample. In order to accurately establish the thermometry location within the sample, a suitable dopant is used and the broadened resonance for that element is observed. The probe neutron flux, after traversing through the sample, is detected with a time of flight (TOF) diagnostic that resolves the neutron energies. In the simplest case, the neutron pulse is created within a negligibly small window in space and in time relative to its flight, *i.e.*, a point-source time spike. In practice, if neutron moderation is required, the moderation time $\tau_{\rm mod}$ introduces uncertainty in the time the neutrons are at the sample and therefore in neutron energy as inferred from the arrival time at the detector. After its birth, the polychromatic neutron pulse spreads along the propagation direction as it flies, and becomes chirped (orderly spread in time, with the highest energy leading). At the TOF diagnostic, the neutrons hit a scintillator and the resulting light is detected over time (and time scales with energy) by a photomultiplier tube (PMT). Typically there are enough neutrons to operate in current mode (rather than single-pulse mode), so that the PMT current is proportional to the neutron-flux rate on the converter.

If the neutron source is going through vacuum, the PMT signal will be a relatively smooth trace that represents the neutron energy distribution (transformed into time) multiplied by instrumental factors. With a resonant material in the path, the neutrons with energy near the resonance scatter, creating a dip in the signal, around a resonant energy value E_R. The width of that dip (the Doppler broadening) can be measured and a temperature can be deduced from it.

The NRS measurement concept using a laser-driven neutron source is illustrated in Fig. 1. The experimental configuration for the NRS measurement in the dynamic material experiment reported in Ref. 9 is sketched in Fig. 2. The actual PMT signals versus time for shocked and unshocked W samples for a 21-eV resonance are shown in Fig. 3. Other resonances have been used; for example, the paper by LeGodec et al.[11] features analysis of the 10.34-eV resonance of $^{181}_{73}Ta$.

II. THEORY BACKGROUND

The slow-neutron scattering resonance cross section for a static nucleus (*i.e.*, describing purely the nuclear effects) has a Lorentzian energy dependence and is given by the Breit-Wigner formula[3,7,12]

$$\sigma_n(E) = \sigma_0 \frac{(\Gamma/2)^2}{(E-E_R)^2 + (\Gamma/2)^2} \tag{1}$$

where the cross section at resonance σ_0 is defined *e.g.* in Refs. 12 and 7, and Γ is the resonance width which is inversely proportional to the lifetime of the virtual level. Values for that resonance cross section

$$\sigma_0 = 4\pi \bar{\lambda_0}^2 g\Gamma_n/\Gamma = \frac{2.604\times10^6}{E_0({\rm eV})}\left(\frac{A+1}{A}\right)^2 \frac{g\Gamma_n}{\Gamma}({\rm barns}),$$

where $\bar{\lambda}_0$ is the de Broglie wavelength of the relative neutron velocity, can be calculated from values for Γ and $g\Gamma_n$ for resonances of atomic number A that are tabulated in Ref. 13 or 14. In Eqn. 1, E_R is the kinetic energy of a neutron in exact resonance, and E is the kinetic energy of the incident neutron. E_R is given by the virtual energy level of the compound nucleus (neutron+target) which is responsible for the occurrence of the resonance plus the energy transferred to the compound nucleus, E_t. In the simplest case, where the target nucleus is free and at rest, E_t is the recoil energy $E_t = mE/(M+m) = E/(A+1)$, where m and M are the masses of the neutron and the target nuclei of atomic number A, respectively. In practice, only in the cross sections at the broad resonances characteristic of light nuclei may the thermal modification of the resonance shape be neglected. That complication can be turned into an advantage by exploiting it for thermometry.

In reality, the scattering involves a neutron moving at velocity $\vec{v}$ in the direction $\hat{z}$ colliding with a nucleus moving with velocity $\vec{V}$. In order to calculate the effective, Doppler-broadened (temperature-modified) cross section, it is useful to define a relative kinetic energy between the neutron and the nucleus, E_r. If we define $V_z \equiv \vec{V}\cdot\hat{z}$ while $v \equiv \vec{v}\cdot\hat{z}$ and assume non-relativistic velocities, then[12]

$$E_r = \frac{1}{2}m(v-V_z)^2 \approx E - mvV_z \tag{2}$$

where terms of order $(V_z/v)^2$ are ignored. The effective Doppler-broadened cross section $\sigma_{\rm eff}$ for a neutron of energy E is given by the convolution of the nuclear cross section with the probability distribution function for V. This distribution can be expressed in general as

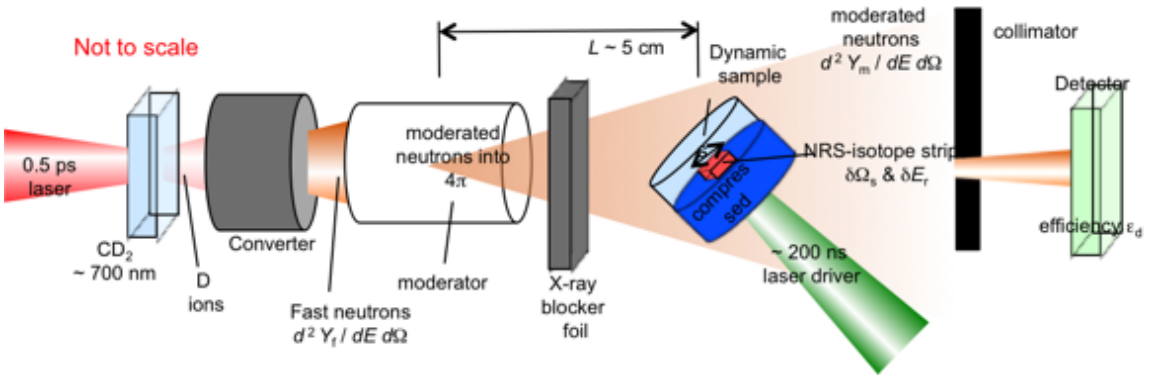

FIG. 1. A not-to-scale diagram of the concept for dynamic NRS with a laser-driven source.

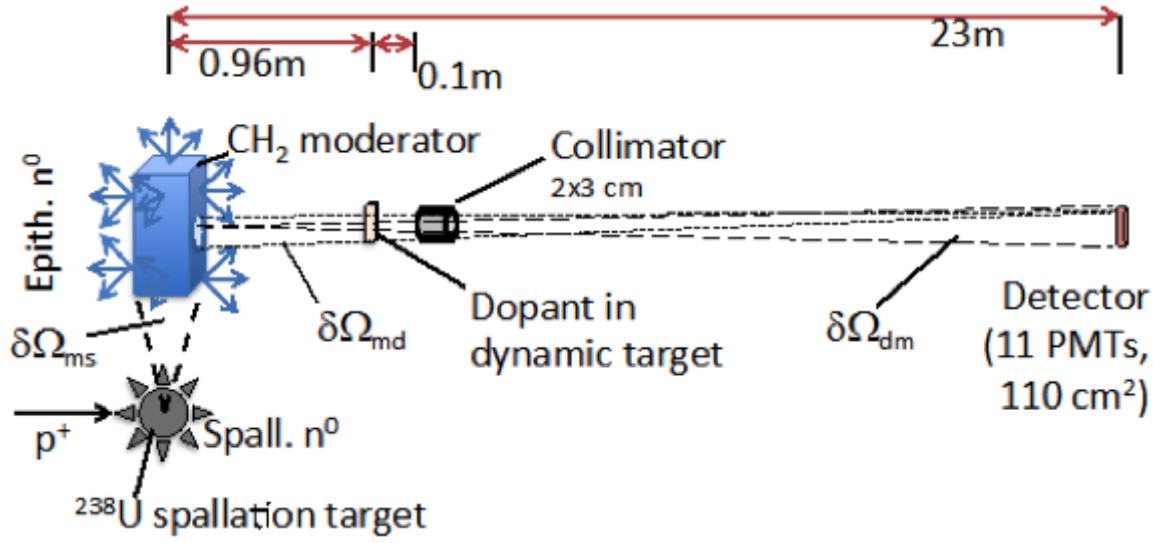

FIG. 2. A not-to-scale diagram of the NRS experimental setup for the dynamic materials experiment carried out at LANSCE, reported in Ref. 9.

$S(E_r)dE_r$ (which integrates to unity). Inserting the relative energy in σ_n, the general expression for the effective cross section is

$$\sigma_{\rm eff}(E) = \int dE_r S(E_r)\sigma_n(E_r) \tag{3}$$

for fixed E. The probability distribution function depends on the environment of the nuclei. Moreover, in the case of dynamic materials, for example, the distribution can have a net velocity ($\langle\vec{V}\rangle \neq 0$), which can be accounted in the data analysis. Hereon, for clarity of exposition in this discussion of measurement accuracy and requirements, we assume the nuclei are on average stationary.

The simplest nuclear environments are either a perfect gas or a classical solid (nuclei treated as harmonic oscillators) bound by Boltzmann statistics, treated in Ref. 12. In that case, the centered MB velocity distribution (no net flow) can be cast as

$$S(E_r)dE_r = \pi^{-1/2}\frac{\exp[-(E_r-E)^2/\Delta^2]}{\Delta}dE_r \tag{4}$$

where

$$\Delta = (4Ek_BT)^{1/2} \approx (4E_Rk_BT)^{1/2} \tag{5}$$

is the Doppler width near the resonance energy and k_B is the Boltzmann constant. Then, the effective cross section is

$$\sigma_{\rm eff}(\varepsilon, E) = \int dE_r S(E_r)\sigma_n(E_r) = \sigma_0\psi(\varepsilon, x) \tag{6}$$

where

$$x = \frac{E-E_R}{\Gamma/2} \tag{7}$$

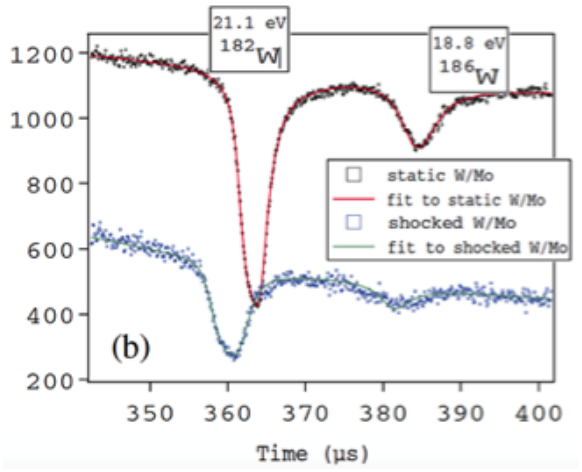

FIG. 3. A TOF PMT signal from the NRS thermometry measurement on dynamic materials experiments from Ref. 9, showing the target resonances to be exploited.

$$\varepsilon = \Gamma/\Delta \tag{8}$$

$$\psi(\varepsilon, x) = \frac{\varepsilon}{2\pi^{1/2}} \int_{-\infty}^{+\infty} \frac{e^{-\frac{1}{4}\varepsilon^2(x-y)^2}}{1+y^2} dy \tag{9}$$

$$y = \frac{E_r - E_R}{\Gamma/2}. \tag{10}$$

$\psi(\varepsilon, x)$ is in general a complicated function of relative energy x with various limits. We highlight a couple of useful limits of this expression:

(a) for ε very large (pure natural width)

$$\psi(\varepsilon, x) = 1/(1+x^2); \tag{11}$$

(b) for ε very small (pure Doppler width) and $x \ll \varepsilon^{-2}$,

$$\psi(\varepsilon, x) = \frac{1}{2}\pi^{1/2}\varepsilon e^{-\frac{1}{4}\varepsilon^2 x^2} = K e^{(E-E_R)^2/\Delta^2} \tag{12}$$

where $K = \frac{1}{2}\pi^{1/2}\varepsilon$. The latter approximation is the most relevant limit for most conceptual MaRIE first experiments trying to measure sample temperature. It is also the approximation used in the pioneering measurement of NRS on dynamic materials in Ref. 9.

The case of nuclei bound in a quantum-mechanical crystal was treated by Lamb many years ago.[15] The quantum-mechanical behavior of a crystal affects the resonance cross section in ways that are not apparent from a study of classical systems. Lamb derived expressions for the probability of creation or annihilation of quanta (phonons) in the various modes of oscillation and used these in an explicit calculation of the resonance shape to be expected if the target nuclei were bound in a Debye crystal. Note that although the Debye model is the solid-state equivalent (phonons in a box) as Plancks law of black body radiation (photons in a box), the energy integral does not diverge because there is a maximum possible phonon frequency ν_m given by a minimum wavelength of twice the atomic separation. The detailed functional dependence of σ_{eff} in this case depends on the temperature relative to the Debye temperature of the crystal, θ_D, which is roughly the temperature at which the mode with the highest-frequency (ν_m) can be excited. To understand the practical implications of these limits, materials with relatively high θ_D include C (2230K), Be (1440K), sapphire (1047K), Si (645K) and Cr (630K). On the other end lie Pb (105K), Au (170K), Sn(200K), Pt and Ta (240K), W (400K), Ni (450K), Al (428K) and Fe (470K). For a cold crystal (relative to the Debye temperature θ_D), and for a sufficiently small neutron resonance width and a fairly low recoil energy (both compared with $k\theta_D$), Lamb showed that a recoilless Breit-Wigner peak could be expected, as well as some crude structure at higher energies. At higher crystal temperatures the usual result is the classical resonance broadening, except that the classical mean energy per degree of freedom, k_BT, in Eqn. 5 must be replaced by the quantum-mechanical mean energy[3,7]

$$\bar{\epsilon} = \frac{1}{2}\int_0^{\nu_m} d\nu h\nu \coth(h\nu/2k_BT) g(\nu) \tag{13}$$

where $g(\nu)$ is the phonon density of states. The mean energy $\bar{\epsilon}$ is greater than k_BT but approaches it asymptotically in the high-temperature limit. This justifies the approximation made in the work in Ref. 9.

Experimentally, one measures the neutron-probe flux through the sample with a density thickness l_0, a density $\rho(l)$ and a fraction $f(l)$ of the dopant material with the desired resonance. The time of flight (TOF) diagnostic is operated in current mode, *i.e.* the current is proportional to the neutron flux. (The neutrons hit a scintillator that makes photons that are in turn detected by a PMT.) Neutrons with energy near E_R are scattered, depleting the current around the time corresponding to the resonant energy. In practice, one measures the attenuation $\alpha(E)$ of the neutron current around E_R, given by[16]

$$\alpha(E) = \int \sigma_{\text{eff}}(E) f(l) \rho(l) dl \tag{14}$$

where hereon the high-temperature limit, and therefore a Gaussian form for σ_{eff}, are assumed. This shape is used to estimate the requirements for an accurate measurement.

Specifically, one wishes to determine k_BT to a given level of accuracy, which may be a specified maximum allowed fractional value $(\delta T/T)_M$ or perhaps a specified maximum uncertainty $(\delta T)_M$ determined over a specified time interval δt.

The NRS thermometry requirements reduce, then, to placing a high enough number of neutrons (N) within the desired area A_s (subtending solid angle $\delta\Omega_s$, as shown in

Fig. 1) and depth l_0 of the sample (assumed to be homogeneous with negligible thermal gradients, as defined by a suitable dopant) over the energy spread of the broadened resonance (Δ) over the specified period δt, to allow a sufficiently accurate fit of the resonance shape to satisfy a thermometry accuracy requirement.

III. DERIVATION OF THERMOMETRY UNCERTAINTY

A. Mathematical idealization of the measurement

Several authors have published data analysis methods and uncertainty analysis with varying levels of detail for NRS thermometry.[17–19] Our discussion here goes into some detail to highlight the choices (experimental and data analysis) that can be made and to derive the uncertainties from the viewpoint of requirements to achieve a desired level of thermometry accuracy.

In general, the neutron source is not spectrally constant. However, for the purposes of our estimations and for clarity, we concern ourselves with the source characteristics very near and around the resonance energy. Although the TOF diagnostic yields a trace of neutron current versus time, for now we work in neutron flux versus neutron energy (E) coordinates, assuming the proper instrumental conversion constants are known and suitably applied.

Per the discussion above, we idealize the TOF PMT detector signal (transformed into a trace versus E) as a constant (proportional to the source neutron flux) minus a Gaussian-shaped function representing the resonant neutron scatter. For the sake of simplicity, we assume all instrumental conversions are divided out and are constant over the width of the resonance, so that without loss of generality, we can set the constant equal to the neutron flux incident on the detector, defined as a_i. We cast the scattered neutron flux (proportional to $\alpha(E)$ of Eqn. 14) in the simplified form $a_s \exp((E-b)^2/(2c^2))$, where a_s is the scattered neutron flux at resonance and $a_s \propto a_i$. To establish the requirements for an optimal (best) case with the minimum neutrons required for a given desired accuracy, we assume that a_s is a constant known precisely, and the uncertainty in the scattered component is dominated by neutron-counting (Poisson) statistics. These approximations are illustrated in Fig. 4. We further assume that the experimental setup can be optimized to make $a_s \equiv a \approx a_i$. The observed signal then $o(E)$ simplifies to

$$o(E) = a_i - a_s \exp(\frac{(E-b)^2}{2c^2}) \tag{15}$$

where all the uncertainty in $o(E)$ is assumed to lie in the Gaussian term, and therefore determined by our ability to fit that term with our observations.

We assume that all the conditions necessary for an accurate fit and for the analytic expressions to be used below are met. These reasonable assumptions are:

- The sampling is complete, *i.e.* we sample an energy interval that encompasses at least 90% of the area under the Gaussian. Unless the resonance lies at very high energy (early time) and is affected by the gamma flash, this condition is easy to satisfy in a TOF diagnostic.

- The sampling rate is constant. That simply requires grouping the data into non-uniform time intervals corresponding to constant energy intervals.

- The sampling interval is near optimal. That means it is large enough to resolve the Gaussian shape, but small enough to keep the statistical uncertainty from Poisson statistics as the dominant one. As an aside, in the case where there is a given, constant uncertainty per sample *e.g.*, an external random noise source of constant amplitude within the resonance energy interval), the variances in the fit parameter are inversely proportional to the sampling interval, *i.e.*, the accuracy gets *worse* if the data are binned into more samples.[20,21] In practice, it is optimal to bin the data so that the energy interval containing 90% of the Gaussian area is covered by ≈ 5 bins. Besides, since neutron moderation will smear to some extent the time-energy correlation, theres no point in having excessively small energy bins with a large fractional variation around the mean energy.

- The maximum likelihood estimate (MLE) formalism is used to fit the Gaussian, so that the Cramer-Rao analytical bounding expressions for the variances in the Gaussian fitting parameters are in fact accurate estimations of said variances.

- All three Gaussian parameters are fit. Although in principle it is possible to regard both a and b as known, in practice it is very hard to know them with arbitrary accuracy.

- For a lower bound on the requirements, we are ignoring the uncertainty in determining the neutron energy (the abscissa uncertainty).

B. Derivation of thermometry accuracy versus neutron count

Under the conditions stated above, the variance in the Gaussian fit parameters are[21,22]

$$(\frac{\delta\Delta}{\Delta})^2 = (\frac{\delta c}{c})^2 = (\frac{\delta b}{c})^2 = \frac{var(c)}{c^2} = \frac{1}{2\sqrt{2\pi}ac} \tag{16}$$

where we note that the variances of b and c are the same, and the resonance Doppler width as defined above is

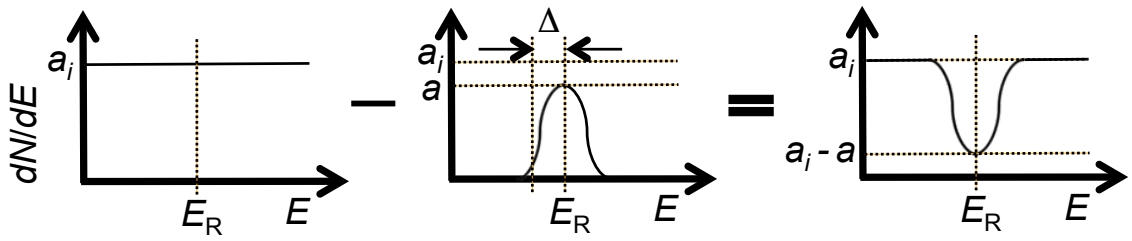

FIG. 4. Idealized form of the TOF signal.

given by $\Delta^2 = 2c^2$. We note that the number of neutrons incident on the detector within the resonance $N_{2\Delta}$ (*i.e.* within the resonant energy interval $\delta E = 2\Delta$) is

$$N_{2\Delta} = 2\sqrt{2}ac. \tag{17}$$

Substituting Eq. 17 into 16 gives

$$\frac{\delta\Delta}{\Delta} = \frac{1}{\pi^{1/4}\sqrt{N_{2\Delta}}}. \tag{18}$$

Taking the derivative of Δ versus T and substituting into Eq.18 yields the fractional uncertainty in temperature

$$\frac{\delta T}{T} = \frac{2}{\pi^{1/4}\sqrt{N_{2\Delta}}} \approx \frac{1.5}{\sqrt{N_{2\Delta}}} \tag{19}$$

where, as expected with Poisson statistics, the temperature uncertainty scales as the square root of the neutrons within the resonance. Therefore, 1% fractional temperature accuracy requires $> 2\times10^4$ neutrons at the detector within the resonance energy width. To gain a quantitative sense, the full Doppler width of the 21-eV resonance in Fig. 3 at 1000 K is $2\Delta \approx 0.34$ eV.

IV. TIME-BASED CONSTRAINTS

The desired thermometry time resolution $\tau_{\rm rsl}$ places a limit on the separation L of the sample from the moderated neutron source. As the neutron bunch flies it spreads out due to the finite kinetic-energy spread. Therefore, the neutrons with the energy spread necessary to cover the resonance will take a certain time interval δt_s to reach the sample rear face. Hereon we neglect the dopant length relative to the flight distance L, to be justified *a posteriori*. We want $\delta t_s \leq \tau_{\rm rsl}$.

To derive the condition for the inequality above to hold, in the expression for the neutron kinetic energy $E = (1/2)m(L/t)^2$ where t is the delay time for the neutron to go from moderator to sample we can solve for time and differentiate versus E to obtain the desired time-resolution condition

$$L \leq \frac{2\tau_{\rm rsl}\sqrt{2E_R/m}}{\delta E/E_R} \tag{20}$$

where $\delta E = 2\Delta$. So to reach a $\tau_{\rm rsl} = 200$ ns time resolution for a generic resonance at $E_R = 21$ eV broadened to a $\delta E = 0.34$ eV, $L < 1.57$ m is needed. For later reference, the neutron flight time for this generic sample resonance energy is 11.8 μs. Since the sample size is ~ 1 cm, neglecting the sample size (and the smaller doped volume) is justified. To restate, even if the energy resolution of our detector is arbitrarily accurate, this separation requirement from TOF stems from the neutrons being able to trace the resonance sufficiently fast, *i.e.*, by enabling the neutrons within the relevant energy spread to sample the dopant before some external condition, such as a decaying shock, changes the sample conditions. Here there is no uncertainty in the measurement *per se*, just in the presumed homogeneity of the sample.

There is a concern of whether the duration of the moderated neutron pulse at birth may smear the measurement time-base (and therefore the neutron energy) enough to impact the measurement accuracy. We start by estimating analytically the effective pulse length of the moderated neutron pulse, τ_n. If the moderator size is l_m, the moderated neutron pulse width is $\tau_n \approx l_m/\sqrt{2E/m}$. To moderate $\sim$ 1 MeV neutrons (typical of the laser-driven source), one needs $l_m \sim 1$ cm, so that $\tau_n \approx 0.2$ μs. (For a brief discussion of the characteristics of a relevant moderated pulse, see Ref. 9.) This effect represents true measurement uncertainty, because the same energy neutrons may be born within the finite time spread of τ_n, and thus represent an irreducible time jitter of the same magnitude at the detector, which translates into an uncertainty in the determination of E. It may seem counterintuitive to seek a 200-ns time accuracy when τ_n is similar. However, although the pulse may be smeared in time, the scattering remains precisely tuned to E regardless of the actual emission time of the neutron from the moderator. As long as $\tau_n \leq \tau_{\rm rsl}$ is satisfied, the moderation energy smearing does not impace the measurement much (see below). If $\tau_n > \tau_{\rm rsl}$, the problem is that the resonance will be sampled outside the desired time-resolution window, possibly adding data from changed sample conditions. Such a situation would require additional remedies, such as a chopping the neutron beam. Since the source-detector distance L_d is different (and larger than L so that the resonance can be spread further in time relative to the fixed τ_n), the finite τ_n imposes

a requirement on the minimum value of L_d. This is the reason why the neutron detector cannot be placed right behind the sample to maximize the neutron flux on it.

To estimate the minimum detector distance to meet a given $\tau_{\rm rsl}$, we use the same derivation as above, this time for L_d and τ_n, and assume that we divide the resonance in B bins, and require the difference in transit time within a bin be larger than τ_n. That yields the minimum separation L_d condition

$$L_d \geq \frac{2B\tau_n\sqrt{2E_R/m}}{\delta E/E_R}. \tag{21}$$

where again $\delta E = 2\Delta$. For $\tau_n = 200$ ns and the generic sample resonance discussed above, the detector placement must be $L_d \geq 3.6$ m. That distance is 6.4× smaller than the $L_d = 23$ m used in the experiments in Ref. 9, which if possible (as in the milder environment of a laser-driven neutron source), would decrease the neutron yield requirement by 40×. Note also the severe penalties in L_d (linear) and necessary neutron yield (quadratic) incurred by overbinning the resonance.

A more precise calculation of the thermometry accuracy taking into account the moderation time requires an accurate Monte Carlo calculation to estimate the shape of the moderated neutron pulse and a formal error analysis of the fit accounting for the uncertainty in E, which lies outside the scope of this paper.

One can shorten this resolution time by placing the (moderated) source closer to the sample, and by going to higher energy resonances. Yuan chose the 21 eV resonance to reduce the transit time for their dynamic experiment; Fowler and Taylor tabulated instead only the 4.16 eV resonance for making their very-long-beamline near-static measurements. This choice becomes a trade-off of relative cross-section, source flux, moderator efficiency, background, and detector efficiency while optimizing the time response. Higher energy may only mean by a factor of ten, or a factor of three in velocity and hence reduction in time. For example, the $^{182}_{74}W$ has resonances at 114 eV (with a huge natural width) and 213 eV (above which the resonances get many and close together).[14] The 213 eV resonance[14] has a $g\Gamma_n = 2.6$ meV which would make it very sensitive. However, the source neutron flux moderated to these higher energies may be exponentially less and insufficient for the available cross-section.

V. GEOMETRIC CONSTRAINTS IN THE MEASUREMENT

A. Geometric setup definitions

Suppose we have a point-like suitably moderated neutron source with differential neutron yield ${dY_m}^2/d\Omega dE$ (see Fig. 1) which integrates over all energies and solid angles to the total number of neutrons N_m. Once the moderator design is optimized to generate as many neutrons as possible near E_R so that the spectral shape is fixed, N_m becomes a source-strength scaling factor. N_m has to be high enough to satisfy the minimum number of neutrons to achieve the desired thermometry accuracy, expressed in the constraint given in Eq. 19, *i.e.*

$$\frac{dY_m(E,\Omega)^2}{d\Omega dE} 2\Delta\delta\Omega_s \geq N_{2\Delta} \tag{22}$$

where $\delta\Omega_s$ is the solid angle subtended by the dopant in the sample located at a separation L. If the source is truly a point, then the active area of the detector (A_d) located at a separation L_d should cover the whole solid angle defined by the target so that

$$A_d = \delta\Omega_s {L_d}^2 \tag{23}$$

and no larger (it does no good). In reality, the detector will be looking at a moderator surface with a finite dimension s_m. In order to increase the signal in that case, the detector size should be increased by $\approx s_m(L_d - L)/L$. If a collimator is placed before the dynamic target, for example to obscure a spallation target or the γ rays from a laser target, the aperture should be large enough to accommodate the finite moderator size.

The moderated-neutron source should be driven by a fast neutron source, such as a state-of-the-art laser-driven neutron source[23,24] or the LANSCE source in Ref. 9, which is our reference here. Each of those sources produces its own fast-neutron spectrum $dY_f(E,\Omega)^2/d\Omega dE$, which integrates to the total number of fast neutrons N_f, to be slowed-down by an optimized moderator.

In general moderators are designed and optimized based on Monte Carlo simulations of neutron transport, and we know of no general analytic approximation to go from Y_f to Y_m. Therefore, in order to evaluate the feasibility of a laser-driven neutron-beam source for thermometry, it is a recommendation of this paper that a first-pass design of a thermometry experiment be done. Once the material, resonance and dimensions are chosen, use a representative laser-driven neutron spectrum (such as in Ref. 24 or others measured subsequently at Trident or at the PHELIX laser in Darmstadt) to design a moderator in order to evaluate the scaling of Y_m with Y_f. That way the required N_f (and laser energy) to satisfy various levels of thermometry accuracy can be determined.

In order to estimate the feasibility of a laser-driven neutron source and to gain insight into the source and experiments in Ref. 9, we examine the latter and do some simple scaling from the latter to the former.

B. Setup with a spallation neutron source at LANSCE

In the configuration for the dynamic material experiments in Ref. 9, shown in Fig. 2, the collimator was essential in order to define the detector field of view and

avoid any view of the spallation target, which would overwhelm the signal. The custom setup in the LANSCE Blue Room was required because the Lujan-Center source and geometry was not suitable for the measurement, yielding a neutron pulse length $\approx 5\times$ longer than the 170 ns realized with the custom setup. To begin the process of generating a neutron pulse, a set of the LANSCE 800-MeV proton micropulses are accumulated in the proton storage ring (PSR). At the desired time, the PSR beam (≈ 5 mC, 2.5×10^{13} protons in a 125-ns pulse) is directed at the spallation target, which generates an approximately isotropic high-energy neutron source of $\approx 5 \times 10^{14}$ spallation neutrons. The multiplication factor of $\approx 20\times$ of incident protons into spallation neutrons is very well established via MCNP modeling benchmarked with experimental measurements. The resulting fast-neutron spectrum Y_f from spallation in that custom setup is not reported. However, it is likely to resemble the one from WNR at 90° in Fig. 2 of Ref. 25. That spectrum has an average neutron energy $E = 8$ MeV. The plastic moderator is a sizeable block placed on top of the spallation source that subtends an effective solid angle $\delta\Omega_{ms}$ when observed from the spallation block center. That geometry determines the fraction of spallation neutrons that the moderator captures. The geometry of the spallation target and moderator assembly is shown below in Fig. 5.

According to MCNP calculations benchmarked experimentally, this configuration results in $S = 1.5 \times 10^{-5}$ moderated neutrons/incident proton/neutron-spectra eV/steradian/cm^2 of moderator area, where the neutrons are emitted into 2π steradians from any point on the moderator surface. The moderator total area is 202 cm^2. Very roughly, over a total ≈ 50 eV window ($\approx 2\times$ the resonance energy), the moderator emits isotropically $\approx 2.4\times10^{13}$ epithermal neutrons. That is consistent with a $\delta\Omega_{ms} \approx 1$ sr, i.e., about 1/10 of the spallation neutrons are captured and down-scattered into this energy window.

In order to quantify the results at the detector end, consider that from any point in the detector, the collimator subtends a solid angle from the detector plane $\delta\Omega_{md} \approx 10^{-6}$ sr, which sets the visible area of the moderator to ≈ 5.2 cm^2. The total detector area is 110 cm^2, which subtends a solid angle from the moderator of $\delta\Omega_{dm} \approx 2\times10^{-5}$ sr (not limited by the collimator). For a spectral width of 300 K (2.7×10^{-2} eV), based on the measured performance, the number of protons, the visible moderator area, and the detector solid angle, we estimate that $\approx 10^3$ neutrons reach the detector over the width of the resonance. This number is not enough for thermometry accurate to 1%. That is consistent with the much larger error bar shown in Ref. 9, although that error bar includes instrumental uncertainties ignored here.

It would be difficult to reproduce the LANSCE NRS setup on MaRIE, as a spallation neutron source so close to an experimental setup presents significant safety issues, diagnostic-noise issues, and geometrical-constraint issues in laser-driven dynamic material experiments, which have much smaller samples and a more compact setup than the HE-driven experiments in Ref. 9. Those motivate consideration of an alternative neutron source with intense short-pulse lasers.

C. Scaling to laser-driven neutron source

As reported in Refs. 23,24, experiments at the LANL Trident laser have utilized a ∼70-J, 0.6-ps laser pulse to drive a deuterium (d+) beam used in turn to produce a forward directed (< 1 sr) fast (average energy $\sim$ MeV) neutron-beam source of $\approx 2 \times 10^{10}$ neutrons born in $\sim$ 1 ns. In this concept, shown in Fig. 1, the laser drives the d+ beam, which is directed at a Be disk (the converter) placed $\sim$ 1 cm farther, where the neutron beam is made by deuteron breakup. The Trident performance is $\sim 100\times$ better than other laser-based efforts and has required the use of an exceptionally high laser-pulse contrast level that in turn allows the utilization of sub-micron thick deuterated plastic-foil laser targets to make a superior deuteron beam, *i.e.*, higher efficiency and higher average energy. The neutron spectrum from the initial Trident experiments[23] has been measured, and the resulting average neutron energy is $\langle E\rangle \approx 2.7$ MeV. That has been decreased to as little as ≈ 0.5 MeV, a fast neutron energy which is $\approx$ 3–16 smaller than the spallation source. The Trident results have been reproduced using the similar PHELIX laser system at GSI in Darmstadt. The neutron-source size demonstrated so far[26] is ≈ 1 mm[26] limited by the conversion geometry. The deuteron-beam diameter at birth is $\approx 10\mu$m, but it diverges in a cone < 1 sr. A desire to protect the converter to avoid Be dispersal has led to a conservatively large target-converter separation limiting the neutron-source size. While not insignificant, the shielding requirements for this miniaturized laser-driven neutron source are much smaller than in Ref. 9.

The level of fast-neutron generating performance demonstrated at Trident (not optimized either experimentally or computationally with a code like MCNP), is comparable to a first-generation neutron-spallation source. However, the neutron yield on Trident is about 4 orders of magnitude below the spallation neutron yield used at LANSCE in Ref. 9. However, a direct comparison can be misleading. Therefore, it is instructive to consider what it would take to provide the same number of epithermal neutrons at the detector over the width of the same resonance in a MaRIE laser-driven dynamic experiment in a miniaturized setup with a laser driven neutron source by scaling from the LANSCE source.

First, only $\approx 1/10$ of the (isotropic) spallation neutrons are incident on the moderator, whereas all of the laser-driven high-energy neutron-beam can be readily captured by a moderator, which gains us one order of magnitude in decreased neutron losses. Second, as explained above, the optimal detector-placement distance is 3.6 m rather

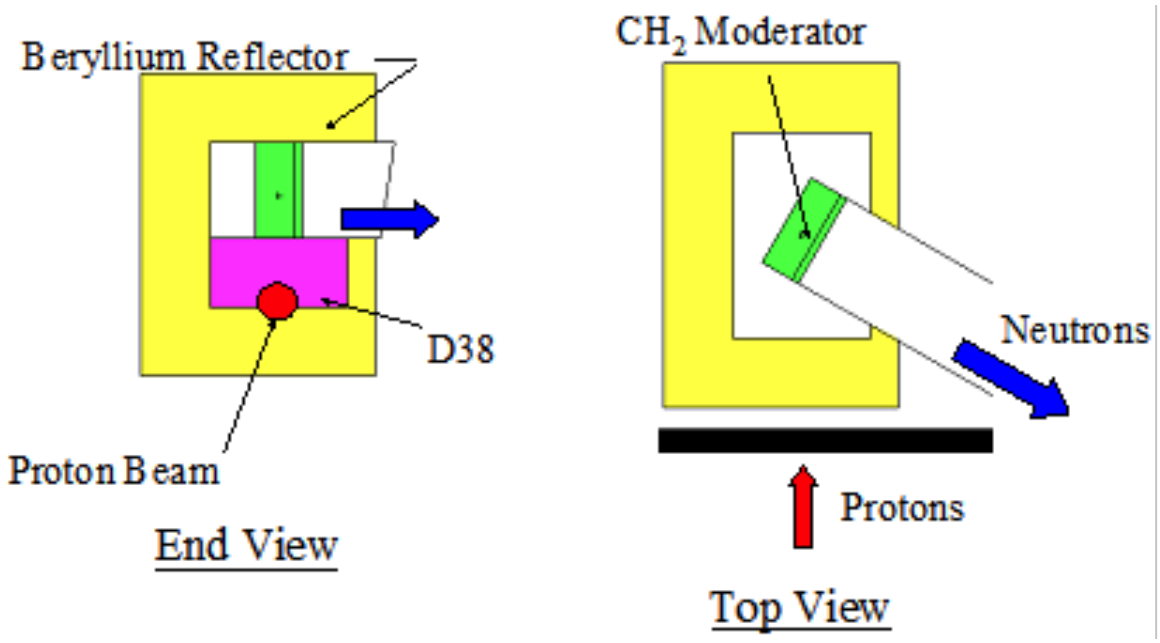

FIG. 5. The combination spallation target / moderator used in Ref. 9. The moderator block dimensions are $3 \times 7.5 \times 7.5$ cm^3, and the spallation block is $2 \times 4 \times 6$ inches^3.

than the 23 m in Ref. 9, which buys another factor of 40 in reduced neutron losses. A laser system does not have the stringent collimation and field of view requirements of a spallation source, so the TOF detector can be brought up to the smaller, optimal distance. LANL scientists in NEN-1 have made great strides in the development of better PMTs for TOF measurements in high-yield pulsed-neutron environments. These are of great potential benefit to MaRIE in this context, although it is hard to estimate the gains from that. Third, the detectors in Ref. 9 saw < 0.1 of the moderator area facing it (5.2 cm^2 / 56 cm^2), and the moderator in a laser system can be made smaller because the laser-produced fast neutrons have much lower energy than the fast spallation neutrons at LANSCE. Without having to worry about viewing the spallation target, the whole moderator can be made visible to the detector in the laser case, which gains us another order of magnitude in sensitivity.

Assuming no further optimization, our rough scaling from LANSCE suggests that thermometry with the same quality can be done with a moderated laser-based neutron-beam source with 4000 $\times$ fewer fast neutrons. Matching that neutron yield would require 2.5$\times$ higher neutron flux than reported on Trident. With no further optimization, that would require (at the same laser intensity) 175 J on target. With present laser technology, such a laser is considerably smaller than the Trident laser and relatively affordable ($\approx$ \$10M from National Energetics of Austin, TX).

There are proposed ways to achieve a neutron yield that is higher by an order of magnitude with the same laser energy as on Trident. One way exploits the steep dependence of neutron yield by d+ breakup versus deuteron energy. That yield scales empirically as $\sim {E_d}^{1.5}$, as shown in Fig. 6, reproduced from Ref. 27. One could increase the average d+ energy $\langle E_d \rangle$ observed on Trident by $> 3\times$ at the same laser energy by using more sophisticated multi-layered targets to reproduce the 18 MeV/nucleon demonstrated with C ions on Trident[28]. Assuming our prior scaling on neutron utilization from the LANSCE experiments is correct, that increased neutron yield could be used to increase the thermometry accuracy beyond what was demonstrated at LANSCE.

D. Monte Carlo calculations of the laser-driven fast neutron production

With a view towards a full forward calculation of an experiment starting with the laser-produced d+ spectrum, the process of fast-neutron generation by d+ breakup was modeled using MCNP6 at LANL, based on the published d+ spectrum from Trident in Ref. 29. The problem is that the relevant nuclear-physics models in MCNP (ISABEL, INCL4, CEM) are intranuclear cascade models developed to serve primarily the high-energy region (100-150 MeV/nucleon), but are often used at lower energies where no evaluated nuclear data are available. Given those shortcomings, the latest version of the TENDL nuclear-data libraries were used and compared to those other existing models. TENDL data libraries are not truly evaluated nuclear data files. It is a nuclear data library which provides the output of the TALYS[30] nuclear code system for direct use in both basic physics and

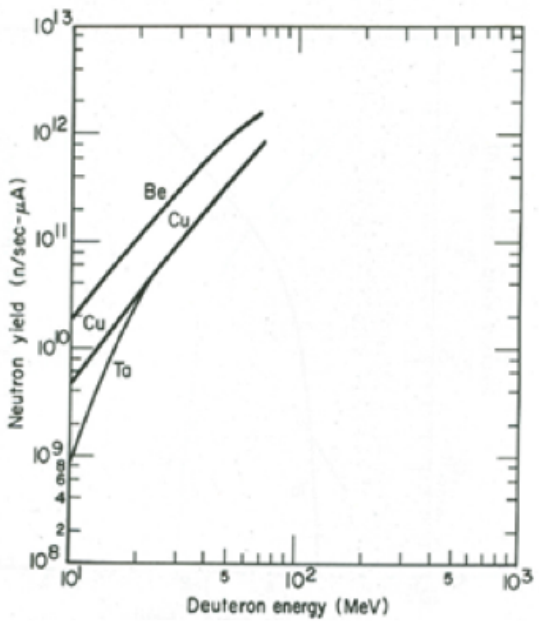

FIG. 6. Neutron yield from d+ breakup in Be versus neutron energy.

applications. TALYS is a deterministic nuclear reaction program for predicting cross sections and other important quantities in the energy region up to 200 MeV (with some extensions up to 1 GeV). TENDL contains data for several incident particles: neutron, proton, deuteron, triton, He-3, alpha and gamma for most isotopes. Therefore, TENDL was deemed as suitable for this study.

The calculation of the neutron spectrum based on the d+ spectrum is done using the MCNP6 code version 6.2 and then the latest version of the TENDL libraries, TENDL-2015. This is the first version of the MCNP6 code that supports data libraries for d+ projectiles. The neutron spectra in TOF detectors at 10, 15, 90, and 160 degrees from the d+ propagation direction are simulated. A table is provided with the integrals of neutron fluxes above 1 MeV, which is a typical threshold for measurements with scintillation detectors. For a case where the forward directed neutron/5e11 d+ was 4.5×10^9, the three cases (TENDL, ISABEL, INCL4) predict values ranging from 1.5 –2.8 $\times10^9$. The difference between the observation and calculations is within the uncertainty in the d+ spectrum that they used. An estimated d+ (improved) spectrum from the multilayer laser target was also run, and is predicted to increase the neutron yield by a factor of a few (which merits closer reexamination). Finally, a variety of candidate neutron-converter materials have bben studied: natural Li, ^{9}Be, ^{12}C, ^{27}Al, ^{59}Co, ^{89}Y, natural W, ^{197}Au, ^{209}Bi, ^{232}Th and natural U. Be is found to perform best, followed by Li, down to 65% of the conversion efficiency of Be.

VI. SUMMARY

We have summarized the concept of bulk (volumetric) thermometry based on neutron resonance spectroscopy (NRS). We have examined the dependence of the measurement on experimental variables and statistics, to relate a desired accuracy level with given sample parameters to constraints on the neutron-source performance and experimental geometry. In general, more compact geometries (smaller moderator-to-sample distances L, Eqn. 20) can achieve faster time resolution. However, epithermal neutrons fly so slowly NRS measurements can never be as fast as the time-scale of some dynamic materials processes. Therefore its use in dynamic experiments must be judicious. NRS can be unconditionally useful for slower temperature measurements such as during processing or manufacturing, or as a high accuracy standard measurement to calibrate other faster indirect methods.

Since the neutron moderator design is done numerically, it is hard to place constraints on the required fast-neutron source from first principles. However, by scaling from the dynamic thermometry experiments demonstrated at LANSCE, we have placed approximate performance requirements on an intense-laser-driven neutron-beam source. Those requirements are very much achievable with present laser technology at a price well within reach of the MaRIE project. As a next step to validate these conclusions and improve this assessment quantitatively, it is recommended that a representative laser-driven neutron spectrum be used to design a moderator for a MaRIE first experiment, and a full forward Monte Carlo calculation with that moderator of a synthetic measurement be done to determine the required fast-neutron yield more accurately. With such a moderator, given availability of a high-intensity high-quality (excellent contrast) ultrafast laser of sufficient energy, an actual temperature measurement should be demonstrated. If successful, such a compact source for NRS could transform the dynamic study of materials.

[1] C. W. Barnes, *Matter-Radiation Interactions in Extremes (MaRIE): Summary of Scientific Functional Requirements (SFRs, Revision 5)*, Tech. Rep. LA-UR-15-28325 (Los Alamos National Laboratory, 2015).

[2] A. Lacerda, A. Migliori, J. C. Fernández, D. Holtkamp, L. Veeser, S. Vogel, L. Smilowitz, G. Rodriguez, S. McGrane, and D. Yarotski, *New Techniques for Dynamic Thermometry*, Tech. Rep. LA-UR-17-22239 (Los Alamos National Laboratory, 2017).

[3] H. E. Jackson and J. E. Lynn, Physical Review **127**, 461 (1962).

[4] P. H. Fowler and A. D. Taylor, in *Neutron Resonance Radiography*, LA-11393-C, edited by J. E. Lynn and D. K. Hyer (Los Alamos National Laboratory, 1987) pp. 46–80.

[5] P. K. Fowler and A. D. Taylor, *Temperature imaging using epithermal neutrons*, Tech. Rep. Report RAL-87-056 (Rutherford-Appleton Laboratory, 1987).

[6] J. C. Frost, P. Meehan, S. R. Morris, R. C. Ward, and J. Mayers, Catalysis Letters **2**, 97 (1989).

[7] H. J. Stone, M. G. Tucker, Y. L. Godec, F. M. Méducin, E. R. Cope, S. A. Hayward, G. Ferlat, W. G. Marshall, S. Manolopoulos, S. A. T. Redfern, and M. T. Dove, Nuclear Instruments and Methods in Physics Research A **547**, 601 (2005).

[8] H. J. Stone, M. G. Tucker, F. M. Méducin, M. T. Dove, S. A. T. Redfern, Y. L. Godec, and W. G. Marshall, Journal of Applied Physics **98**, 064905 (2005).

[9] V. W. Yuan, J. D. Bowman, D. J. Funk, G. L. M. R. L. Rabie, C. E. Ragan, J. P. Quintana, and H. L. Stacy, Physical Review Letters **94**, 125504 (2005).

[10] D. C. Swift, V. W. Yuan, R. G. Kraus, J. M. McNaney, D. P. Higginson, A. MacKinnon, F. Beg, K. Lancaster, and H. Nakamura, in *Shock Compression of Condensed Matter – 2011*, Vol. 1426, AIP Conference Proceedings (American Institute of Physics, 2012) p. 376.

[11] Y. LeGodec, M. T. Dove, D. J. Francis, S. C. Kohn, W. G. Marshall, A. R. Pawley, G. D. Price, S. A. T. Redfern, N. Rhodes, N. L. Ross, P. F. Schofield, E. Schooneveld, G. Syfosse, M. G. Tucker, and M. D. Welch, Mineralogical Magazine **65**, 737 (2001).

[12] H. A. Bethe, Reviews of Modern Physics **9**, 69 (1937).

[13] S. F. Mughabghab, M. Divadeenam, and N. E. Holden, *Neutron Resonance Parameters and Thermal Cross Sections Part A $Z = 1 - 60$*, edited by S. F. Mughabghab, R. R. Kinsey, and C. L. Dunsford, Neutron Cross Sections, Vol. 1 (Academic Press, New York, 1981).

[14] S. F. Mughabghab, *Neutron Resonance Parameters and Thermal Cross Sections Part B $Z = 61 - 100$*, edited by S. F. Mughabghab, R. R. Kinsey, and C. L. Dunsford, Neutron Cross Sections, Vol. 1 (Academic Press, New York, 1981).

[15] W. E. Lamb, Physical Review **55**, 190 (1939).

[16] D. C. Swift, A. Seifter, D. B. Holtkamp, V. W. Yuan, D. Bowman, and D. A. Clark, Physical Review B **77**, 092102 (2008).

[17] J. Mayers, G. Baciocco, and A. C. Hannon, Nuclear Instruments and Methods in Physics Research A **275**, 453 (1989).

[18] D. P. Higginson, J. M. McNaney, D. C. Swift, T. Bartal, D. S. Hey, R. Kodama, S. Le Pape, A. Mackinnon, D. Mariscal, H. Nakamura, N. Nakanii, K. A. Tanaka, and F. N. Beg, Physics of Plasmas **17**, 100701 (2010).

[19] M. Gu, H. Fang, B. Liu, X. Liu, S. Huang, C. Ni, Z. Li, and R. Wang, Nuclear Instruments and Methods in Physics Research B **269**, 528 (2011).

[20] N. Hagen, M. Kupinski, and E. L. Dereniak, Applied Optics **46**, 5374 (2007).

[21] W. contributors, "Gaussian function — wikipedia, the free encyclopedia," (2017), [Online; accessed 13-December-2017].

[22] D. A. Landman, R. Roussel-Dupré, and G. Tanigawa, The Astrophysical Journal **261**, 732 (2007).

[23] M. Roth, D. Jung, K. Falk, N. Guler, *et al.*, Physical Review Letters **110**, 044802 (2013).

[24] J. C. Fernández, D. C. Gautier, C. Huang, S. Palaniyappan, *et al.*, Physics of Plasmas **24**, 056702 (2017).

[25] S. F. Nowicki, S. A. Wender, and M. Mocko, in *Conference on the Application of Accelerators in Research and Industry, CAARI 2016, 30 October – 4 November 2016, Ft. Worth, TX, USA*, Physics Procedia, Vol. 90 (Elsevier, 2017) p. 374.

[26] N. Guler, P. Volegov, A. Favalli, F. E. Merrill, K. Falk, D. Jung, J. L. Tybo, C. H. Wilde, S. Croft, C. Danly, O. Deppert, M. Devlin, J. Fernandez, D. C. Gautier, M. Geissel, R. Haight, C. E. Hamilton, B. M. Hegelich, D.Henzlova, R. P. Johnson, G. Schaumann, K. Schoenberg, M. Schollmeier, T. Shimada, M. T. Swinhoe, T. Taddeucci, S. A. Wender, G. A. Wurden, , and M. Roth, Journal of Applied Physics **120**, 154901 (2016).

[27] A. Rindi, *Neutron Production from Heavy Ion Interaction: some very empirical considerations*, Tech. Rep. LBL-4212 (Lawrence Berkeley National Laboratory, 1975).

[28] S. Palaniyappan, C. Huang, D. C. Gautier, C. E. Hamilton, M. A. Santiago, C. Kreuzer, A. B. Sefkow, R. C. Shah, and J. C. Fernández, Nature Communications **6**, 10170 (2015).

[29] D. Jung, K. Falk, N. Guler, O. Deppert, M. Devlin, A. Favalli, J. C. Fernández, D. C. Gautier, M. Geissel, R. Haight, C. E. Hamilton, B. M. Hegelich, R. P. Johnson, F. Merrill, G. Schaumann, K. Schoenberg, M. Schollmeier, T. Shimada, T. Taddeucci, J. L. Tybo, S. A. Wender, C. H. Wilde, G. A. Wurden, , and M. Roth, Physics of Plasmas **20**, 056706 (2013).

[30] A. J. Koning and D. Rochman, Nuclear Data Sheets **113**, 2841 (2012).